

Theoretical study on RbCl crystal with Möbius inverse potentials

Yue Shen, Shuo Zhang, and Nan-xian Chen

Department of Physics, Tsinghua University, Beijing, 100084, China

Abstract

The alkali halides have been studied very frequently for their simple structures and interesting properties, for example, the high-pressure induced transition¹. There are several successful models that can be employed. The most famous model of them is the Tosi-Fumi interionic potential² which is an empirical potential derived from the experimental data. Whereas, here we developed a new potential model based on the Möbius lattice inversion method^{3,4}, which can be derived directly from the cohesive energy curve without any experimental data and is more effective than the ab initio calculation. With the Möbius interionic potentials, we calculated the structural and elastic properties of RbCl crystal. The results are in good agreement with experiments. We also studied the high-pressure induced B1-B2 transition of RbCl crystal and estimated approximately the transition-point which is about 1.09GPa. Further more, we used this potential model to simulate the RbCl melting with molecular dynamics. The calculated melt-point is approximately 990K~995K, close to the experimental data.

Key words:

PACS:

1 Introduction

During the past 60 years the alkali halides have been well studied for their thermodynamic, elastic and structural properties. The Tosi-Fumi potential model² is usually employed. Among those available models that can correctly describe the alkali halides, the pairwise interionic potentials always include two parts: the long-range Coulomb term and the short-range term. The Coulomb term is of the form $Z_i Z_j / r_{ij}$, where r_{ij} represents the distance between the i th and the j th ions, Z_i and Z_j represent their effective charges. While there is not a definitive form of the short-range term. Tosi-Fumi model uses the forms

as

$$-\frac{C_{ij}}{r_{ij}^6} - \frac{D_{ij}}{r_{ij}^8} + A_{ij} \exp(-B_{ij} r_{ij})$$

, which represent dipole-dipole, dipole-quadrupole, and repulsion terms respectively. However, if we have the short-range potential curves, any compatible function forms will be fitted to the potential curves with adaptive parameters. In previous models² the parameterization of potentials is usually obtained by empirical fitting which depends on experimental data. These empirical potentials are only applicable with certainty over the range of interionic distances used in the fitting procedure, which may lead to problems if the potential is used in a calculation that accesses distances outside this range. Here we find the way based on the Möbius lattice inversion method to avoid these problems. Using the lattice inversion method we get the short-range potential curves solely from the cohesive energy curves which can be calculated with quantum mechanics. It is to say that our short-range potential curves are derived without any experimental data. This method will be discussed in detail later. Another question is how to define the effective charges of cations and anions. One possible choice is to assign cations and anions with formal charges as Rb+1 and Cl-1. But here we use another way to decide the effective charges which is depicted in part II. We consider nonintegral charges are more reasonable. This paper is organized as follows: First, we introduce our Möbius inverse potential model in detail. Further, some structural and elastic properties of B1-RbCl crystal are calculated and compared with experimental data. Second, we study the high-pressure-induced transition from B1 structure to B2 structure with our model, the transition point is also provided. Finally, we simulate the melting of B1-RbCl crystal with molecular dynamics employing our model and calculate the correct melting temperature with a coexist-phase method. Thus we come to the conclusion that our Möbius inverse potential model is successful in describing the RbCl alkali halide and this lattice inversion technique should have a wider perspective.

2 Möbius inverse pairwise interionic potentials

The main idea of Möbius lattice inversion method can be described simply as follows^{5,6}: For a single element crystal, the cohesive energy can be expressed as

$$E(x) = \frac{1}{2} \sum_{n=1}^{\infty} r_0(n) \phi(b_0(n)x) \quad (1)$$

where x is the nearest-neighbor distance, $r_0(n)$ is the n th neighbor, and $\phi(x)$ is the pair potential. By a self-multiplicative process from $\{b_0(n)\}$, the $\{b(n)\}$ is formed, a multiplicative closed semi-group. This implies that a lot of virtual lattice points are involved, but the corresponding virtual coordination number

is zero. In the $\{b(n)\}$, for any two integers m and n , there is a sole integer k such that $b(k) = b(m)b(n)$. Hence, the equation above can be rewritten as

$$E(x) = \frac{1}{2} \sum_{n=1}^{\infty} r(n)\phi(b(n)x) \quad (2)$$

where

$$r(n) = \begin{cases} r_0(b_0^{-1}[b(n)]), & b(n) \in \{b_0(n)\} \\ 0, & b(n) \notin \{b_0(n)\} \end{cases} \quad (3)$$

Then the general equation for the pairwise interatomic potential obtained from Möbius inversion can be expressed as

$$\phi(x) = 2 \sum_{n=1}^{\infty} I(n)E(b(n)x) \quad (4)$$

where $I(n)$ has the characteristics of

$$\sum_{b(d)|b(n)} I(d)r\left(b^{-1}\left[\frac{b(n)}{b(d)}\right]\right) = \delta_{n1} \quad (5)$$

Thus we get the pair potential just from the cohesive energy curve. But we encounter some obstacles when we try to get the interionic pair potentials from the B1-RbCl cohesive energy curve. First, we have to know the effective charges of cations and anions so that we can remove the Coulomb energy from the total energy and remain only the short-range terms. Then we use Möbius lattice inversion to obtain the short-range potentials from the so called short-range-energy curve. However, there are still three types of short-range potentials as Rb-Rb, Rb-Cl, Cl-Cl, and it is impossible to find a lattice constructed only with one kind of ion. To solve this problem we build several virtual structures of lattice that may be not real for RbCl crystal. These virtual structures have some similar traits with the real B1-structure. For example, one of them, the B3 structure has the same sublattice of Rb-Rb and Cl-Cl with the B1 structure. That means the B3 structure contains the same contributions of cation-cation interaction and anion-anion interaction with the B1 structure. When the short-range-energy curve of the B1-structure is subtracted by that of the B3-structure, we clearly get the energy that contains only the contribution of cation-anion interaction and its relationship with lattice constant.

The total energies of B1, B3, T1, and B2 structures are calculated with CASTEP^{7,8,9} (Cambridge Serial Total Energy Package). The ultra-soft pseudopotentials for rubidium and chlorine ions are adopted and the GGA-PW method is used to cope the exchange-correlation energy. And the k-mesh points over Brillouin zone are generated with parameters $4 \times 4 \times 4$ for the biggest reciprocal space and $1 \times 1 \times 1$ for the smallest one by the Monkhorst-Pack-scheme¹⁰ corresponding to lattice constant a . The energy tolerance for SCF

convergence is 2×106 eV/atom, and the kinetic energy cutoff for plane wave basis set is 260 eV.

To decide the effective charges we process as follows: Since the short-range parts are quickly convergent when the lattice constant increases, the total contribution of energy with the lattice constant larger than 10.0 \AA is almost completely from the Coulomb part. Then, by using the Madelung constants of B1 and B3-structure¹¹ we can determine the effective charges of ions from the energy difference between the total energies of B1 and B3-structure RbCl crystals of large lattice constant.

After having known the effective charges we may calculate the Coulomb energies of different structures employing the Ewald summation¹² and remove this part of energy from the total cohesive energy. Then we start the lattice inversion from the short-range-energy curve.

For B1-structure

$$E_{SR}^{B_1}(a) = E_{++}^{B_1}(a) + E_{--}^{B_1}(a) + E_{+-}^{B_1}(a) + E_i \quad (6)$$

where ESR means the short-range parts of the total energy, E_{++} , E_{--} and E_{+-} are the energy contributions of cation-cation, anion-anion and cation-anion respectively, E_i refers to the energy of an isolated ion, and a is the lattice constant. All energy terms are averaged to each ion. Further we have

$$E_{++}^{B_1}(a) = \frac{1}{4} \sum_{i,j,k \neq 0} \phi_{++} \left(\frac{a}{2} \sqrt{(i+k)^2 + (i+j)^2 + (j+k)^2} \right) \quad (7)$$

$$E_{--}^{B_1}(a) = \frac{1}{4} \sum_{i,j,k \neq 0} \phi_{--} \left(\frac{a}{2} \sqrt{(i+k)^2 + (i+j)^2 + (j+k)^2} \right) \quad (8)$$

$$E_{+-}^{B_1}(a) = \frac{1}{2} \sum_{i,j,k \neq 0} \phi_{+-} \left(\frac{a}{2} \sqrt{(i+k-1)^2 + (i+j-1)^2 + (j+k-1)^2} \right) \quad (9)$$

Where ϕ_{++} , ϕ_{--} , and ϕ_{+-} are the short-range interionic potentials of cation-cation, anion-anion and cation-anion respectively.

For B3-structure

$$E_{SR}^{B_3}(a) = E_{++}^{B_3}(a) + E_{--}^{B_3}(a) + E_{+-}^{B_3}(a) + E_i \quad (10)$$

and

$$E_{++}^{B_3}(a) = \frac{1}{4} \sum_{i,j,k \neq 0} \phi_{++} \left(\frac{a}{2} \sqrt{(i+k)^2 + (i+j)^2 + (j+k)^2} \right) \quad (11)$$

$$E_{--}^{B_3}(a) = \frac{1}{4} \sum_{i,j,k \neq 0} \phi_{--} \left(\frac{a}{2} \sqrt{(i+k)^2 + (i+j)^2 + (j+k)^2} \right) \quad (12)$$

$$E_{+-}^{B_3}(a) = \frac{1}{2} \sum_{i,j,k \neq 0} \phi_{+-} \left(\frac{a}{2} \sqrt{(i+k-\frac{1}{2})^2 + (i+j-\frac{1}{2})^2 + (j+k-\frac{1}{2})^2} \right) \quad (13)$$

As we can see, the difference is just between the cation-anion interactions.

So we have

$$\begin{aligned} \Delta E_{+-}^{SR}(a) &= E_{SR}^{B_1}(a) - E_{SR}^{B_3}(a) \\ &= E_{+-}^{B_1}(a) - E_{+-}^{B_3}(a) \\ &= \frac{1}{2} \sum_{i,j,k \neq 0} \phi_{+-} \left(\frac{a}{2} \sqrt{(i+k-1)^2 + (i+j-1)^2 + (j+k-1)^2} \right) \\ &\quad - \frac{1}{2} \sum_{i,j,k \neq 0} \phi_{+-} \left(\frac{a}{2} \sqrt{(i+k-\frac{1}{2})^2 + (i+j-\frac{1}{2})^2 + (j+k-\frac{1}{2})^2} \right) \end{aligned} \quad (14)$$

Note that the isolated-ion energy is also gone.

This equation may be rewritten as

$$\Delta E_{+-}^{SR}(x) = \frac{1}{2} \sum_{n=1}^{\infty} R_{+-}(n) \Phi_{+-}[B_{+-}(n)x] \quad (15)$$

in which we substitute lattice constant a with the nearest cation-anion distance x . Then we follow the way discussed at the beginning of this part to obtain the curve of $\Phi_{+-}(x)$. The derivation of cation-cation and anion-anion short-range potentials is of the same manner. For instance, in order to extract the anion-anion short-range interaction we build a T1-structure lattice. The T1-structure lattice has the same sublattice of Rb-Rb with B1-structure. So the short-range energy difference between those two structures is dedicated by the cation-anion and the anion-anion interactions and we can exclude the cation-anion part since the cation-anion interionic potential is already known. For the cation-cation one we simply use the B2 and B1-structure lattices, extract the cation-cation interaction with the cation-anion and the anion-anion potentials available. The whole process can be illustrated in Fig.1. After all the short-range-potential curves are attained, we use several forms of functions to fit these curves and get the suited parameters. We choose an exponential repulsive function for cation-anion and a Morse-stretch function for anion-anion. We find that among the three short-range potentials the cation-anion one is excessively more important than the other two while the cation-cation one is much smaller even than the anion-anion's, almost can be neglected. This leads us to ignore the cation-cation short-range interaction for saving calculation time.

Rb-Cl			Cl-Cl			Effective	Charges
$D_{+-}(ev)$	$R_{+-}(\text{\AA})$	γ_{+-}	$D_{--}(ev)$	$R_{--}(\text{\AA})$	γ_{--}	q_+	q_-
1.8140	2.4470	6.7525	0.1508	3.8632	8.5640	0.96930e	-0.96930e

Table 1

Parameters of potential functions

So the potentials can be expressed as

$$\Phi_{+-}(x) = D_{+-} \exp \left[\gamma_{+-} \left(1 - \frac{x}{R_{+-}} \right) \right] + \frac{q_+ q_-}{4\pi\epsilon_0 x} \quad (16)$$

$$\Phi_{--}(x) = D_{--} \left(\left\{ 1 - \exp \left[\gamma_{--} \left(1 - \frac{x}{R_{--}} \right) \right] \right\}^2 - 1 \right) + \frac{q_- q_-}{4\pi\epsilon_0 x} \quad (17)$$

$$\Phi_{++}(x) = \frac{q_+ q_+}{4\pi\epsilon_0 x} \quad (18)$$

The potential parameters for RbCl are listed in Table I.

With this potential model we calculate some structural and elastic properties of B1-RbCl crystal at 0K. The results are listed in Table II. Compared with experimental data at room temperature¹³, the results show a good agreement.

3 High-pressure-induced B1-B2 transition

Most alkali halides crystallize in the B1 (NaCl-like) structure under ambient temperature and pressure but turn into the B2 (CsCl-like) structure under a highly external hydrostatic pressure. Since Slater¹ first described this phase transition in 1924, it has been considered to be one of the simplest first-order transitions of alkali halides. However, its mechanism still remains uncertain¹⁴. If we restrict this transition to a single-step process without intermediate structures¹⁵, there are some mechanisms that may be taken into account. One of them is the Buerger mechanism¹⁶, according to which pressure contracts the B1 primitive rhombohedral cell along the [111] axis, leading to the B2 phase. Another one is proposed as the WTM mechanism¹⁷ that concerns with the relative displacement of consecutive [100] planes. The third mechanism¹⁸ is closely related to the Buerger one and concerns with the orientational relations in a pressure-induced transition.

In our present work, we do not want to discuss the mechanism so we just select the Buerger mechanism for its simplicity. We try to explain the reason of transition using the energy minimization technique. Here we introduce the Gibbs free energy $G=U+PV$, to represent the total crystal energy, where U refers to

the whole cohesive energy (including the Coulomb part and the short-range parts), P is the external pressure, V is the lattice volume, and PV indicates the contribution of external pressure. We don't consider the temperature factor, so that all the calculations are under absolute zero.

Due to its too many freedom-degrees, the Gibbs free energy surface is a hypersurface that can not be drawn on a 2-dimension plane. However, we may fix the symmetry of the primitive cell as $R\bar{3}m$, change the lattice constant simultaneously with the rhombohedral angle along the B1-B2 transition path, as described in the Buerger mechanism. Then make the lattice constant as X-coordinate, the rhombohedral angle as Y-coordinate and the Gibbs free energy as the function of both lattice constant and rhombohedral angle. Thus we can draw the Gibbs free energy surface with a 2-dimension expression.

The Gibbs free energy surface at zero pressure is shown in Fig.2 (a). From the scheme we can see at zero pressure the B1 and B2-structure are both local minima which mean stable and obviously the B1-structure has a lower energy position than the B2-structure. When we add an external pressure to the cell, the whole energy surface will rise and the B1 minimum rises faster relatively to the B2 minimum. But the B1 minimum remains lower than the B2 minimum until the external pressure is high enough and then a phase transition may occur. For this reason, we can expect the B1-structure to be a more stable structure than the B2-structure under a external pressure beneath the transition-pressure.

In order to find the transition-point we calculate the Gibbs free energies of relaxed B1 and B2-structure at different external pressures by energy minimization. Both Gibbs free energies increase with the external pressure and they have one crosspoint at about 1.09GPa, beneath this value of pressure, the Gibbs free energy of B1-structure is lower than that of B2-structure, while above this value, the situation is just the opposite, as shown in Fig.3. It indicates that, at an external pressure above 1.09GPa, the B2-structure is more stable than B1, so the transition-point is approximately 1.09GPa. This estimated transition-point accords well with the experimental data about 10kbar in Ref.13.

From the Gibbs free energy surface at the transition pressure, shown in Fig.2 (b), we can see the B1 and B2 minima are of the same depth which means the B1 and B2-structure are of the same stability at this time. However, it is difficult for a B1-structure to turn into a B2-structure spontaneously by energy minimization because there is still an energy barrier between the two minima. With the further increase of external pressure the B1 minimum will become higher and higher. Finally, the B1-structure will turn to a saddle point while the B2-structure remains a minimum and there is clearly a downhill path from B1 to B2, as shown in Fig.2 (c). Then we may achieve the process from B1-B2

using the energy minimization method.

4 Molecular dynamic simulation of RbCl melting

To perform our model to the thermal properties of B1-RbCl we employ a MD technique. A detailed description of the molecular dynamics method may be found elsewhere¹⁹. In our work, the simulations are performed using the MSI dynamics engine²⁰. The successful runs rely on the size of system (number of particles N), size of timestep (Δt), the total running time (total steps of run n_{steps}), as well as the parameters of the temperature and pressure control methods. After some test runs we find the correct results can be obtained with $N = 512$, $\Delta t = 5$ fs, $n_{steps} = 10000$. And we choose Hoover method to control the temperature and Andersen method to control the pressure exactly at 0GPa. The NPT (constant N is the number of particles, T is the temperature and P is pressure) ensemble is adopted.

First we simulate the thermal expansion of B1-RbCl below the melting point. The volume-temperature curve is shown in Fig.4. We also approximately calculate the linear coefficient of thermal expansion α at different temperatures, listed in Table III. Compared with the experimental data¹³, the calculated values are reasonable.

However, we encounter a discrepancy when we try to decide the melt-point by heating the perfect lattice until it melts. The abrupt change of volume which indicates the solid-liquid transition occurs at the temperature of about 1260K, much higher than the real melting temperature T_m 988K¹³. And the lattice remains solid at the temperature under which it is expected to have been melted. This over-heat problem has been discussed in some papers^{21,22,23}. It is said that the calculated melt-point with a perfect lattice as the initial configuration will be somewhat larger than the real melt-point, even larger by an amount of the order of 20-30%²¹. And it is caused by the lack of nucleation sites for the liquid phase as the crystal is heated.

To avoid the over-heat problem and get the correct melt-point we use a coexist-phase lattice as the initial configuration^{22,23}, which means half of the particles are solid and the rest are liquid. This coexist-phase lattice can be obtained in the following manner: First, we build a superlattice of 512 particles (256 Rb+ and 256 Cl- respectively). Then, with half of the particles fixed, a MD run is carried out at a high enough temperature to make sure the movable part can completely melt. Thus the coexist-phase lattice with a common interface of the solid part and the liquid part is obtained, as shown in Fig.6 (a). Using this coexist-phase lattice as the initial configuration, a series of MD runs at different temperatures are performed and the final configurations are

saved and analyzed. We find the abrupt change of volume happens at about 995K, very close to the real melting temperature, as shown in Fig.5. From the saved trajectory files we calculate the radial distribution function (RDF) and the mean-square displacement (MSD) of the final configurations at different temperatures. The abrupt changes of RDF and MSD also indicate the occurrence of melting, as shown in Fig.7, Fig.8. Further more, we pick up two final configurations which represent complete-solidification and complete-melting as shown in Fig.6 (b), (c). We can see the final configurations are disparate on two sides of the melt-point even though they have the same initial configurations. For comparison, the V-T curve with a perfect lattice as the initial configuration is also shown in Fig.5. The difference between the two calculated "melt-point" is about 260K. So we prefer the coexist-phase method as the correct method to calculate the melt-point of RbCl.

The MD simulations above are all carried out at 0 GPa. With an external hydrostatic pressure adding to the superlattice, a more serious over-heat problem will have to be taken into account. Detailed discussion can be found in Ref.23.

Actually, the calculated "melt-point" with an initial configuration of perfect lattice is not a denotation of melting, but of the mechanical instability of the chosen model. One must be sure not to confuse with these two conceptions.

5 Conclusion

Based on the Möbius inverse potential model, we have studied the static structural and elastic properties of B1-RbCl crystal. The calculated value are in good agreement with experimental data. The high-pressure-induced B1-B2 transition of RbCl crystal is also studied. The estimated transition-pressure is about 1.09GPa, consistent with experimental data¹³. Using the MD technique we have simulated the melting of RbCl crystal at 0GPa and calculated the correct melt-point with a coexist-phase method.

For these applications of the Möbius inverse potentials, we consider it as a reliable model although it is derived just from the cohesive energy curve without any empirical data employed.

However, there are still some defects in our model. First, using the Möbius inversion method can only obtain the pairwise potential, so that we must add a 3-body or more potential when it is needed²⁴. Second, due to the infinite terms of summation as , a quickly convergent $E(x)$ is demanded. That is the reason why we need to remove the Coulomb part from the total cohesive energy while dealing with the ionic crystals.

Despite these flaws, we can see the simplicity and validity of this Möbius lattice inversion method. This method has successfully been used to obtain the interatomic potentials in rare-earth metals and intermetallic compounds²⁵, and now the interionic potentials of alkali halides.

Acknowledgements

Thanks for financial support from the National Nature Science Foundation of China and the National Advanced Materials Committee of China. Special support from the 973 Project in China, No.G2000067101, is hereby acknowledged.

References

- [1] J.C. Slater, Phys. Rev. 23, 488 (1924)
- [2] M.P. Tosi and F.G. Fumi, J. Phys. Chem. Solids 25, 45 (1964).
- [3] Maddox J, Nature 344, 377 (1990)
- [4] N.X. Chen, Phys. Rev. Lett. 64, 1193 (1990)
- [5] N.X. Chen, Z.D. Chen, and Y.C. Wei, Phys. Rev. E 55, R5 (1997)
- [6] N.X. Chen, X.J. Ge, W.Q. Zhang, and F.W. Zhu, Phys. Rev. B 57, 14203 (1998)
- [7] CASTEP, Molecular Simulation Software (1998)
- [8] I. Yoji, M. Masakazu, and T. Tatsuo, Thin Solid Films 381, 176(2001)
- [9] <http://www.accelrys.com/cerius2/castep.html>
- [10] H.J. Monkhorst and J.D. Pack, Phys. Rev. B 13, 5188(1976)
- [11] C. Kittel, Introduction to Solid State Physics, John Wiley and Sons, p.66-72, (1996)
- [12] P.P. Ewald, Ann. Phys. 64, 253 (1921)
- [13] D.B. Sirdeshmukh, L. Sirdeshmukh, K.G. Subhadra, Alkali halides: a handbook of physical properties (Berlin; New York: Springer, 2001)
- [14] M.A. Blanco, A. Costales, A. Martín Pendás, and V. Luña, Phys. Rev. B 62, 12028 (2000)
- [15] S. Kelly, R. Ingalls, F. Wang, B. Ravel, and D. Haskel, Phys. Rev. B 57, 7543 (1998)

- [16] M.J. Buerger, in Phase Transformation in Solids, edited by R. Smoluchowski, J.E. Mayer, and W.A. Weyl (Wiley, New York, 1951), pp. 183-211
- [17] M. Watanabe, M. Tokonami, and N. Morimoto, *Acta Crystallogr., Sect. A: Cryst. Phys., Diffr., Theor. Gen. Crystallogr.* 33, 294 (1977)
- [18] B. Okai, *J. Phys. Soc. Jpn.* 48, 514 (1980)
- [19] M.P. Allen and D.J. Tildesley, *Computer Simulation of Liquids* (Clarendon, Oxford, 1987)
- [20]
 - http://www.accelrys.com/doc/materious/cerius40/FFBSim/5_Dynamics.html#302888
- [21] Furio Ercolessi, *A Molecular Dynamics Primer* (Spring College in Computational Physics, ICTP, Trieste, June 1997)
- [22] J.R. Morris, C.Z. Wang, K.M. Ho, and C.T. Chan, *Phys. Rev. B* 49, 3109 (1994)
- [23] A.B. Belonoshko, R. Ahuja, and B. Johansson, *Phys. Rev. B* 61, 11928 (2000)
- [24] Y. Liu, N.X. Chen, and Y.M. Kang, *Mod. Phys. Lett. B* 16, 187(2002)
- [25] N.X. Chen, J. Shen, and X.P. Su, *J. Phys.: Condens. Matter* 13, 2727 (2001)

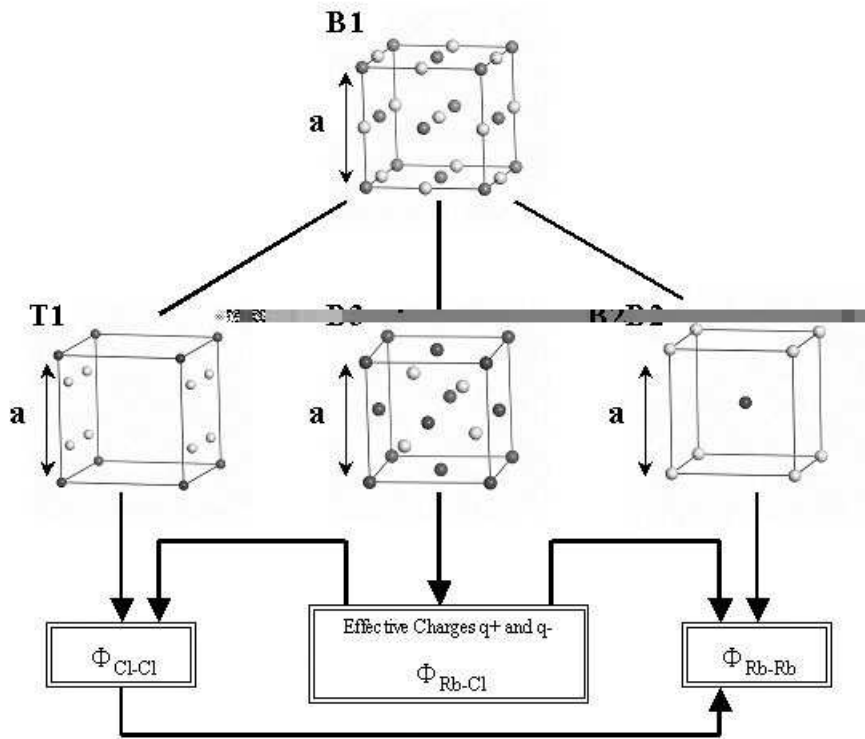


Fig. 1. The derivation of Möbius interionic potentials. Three types of virtual structure are constructed: B3, T1, and B2, for the purpose of extracting one from the totally three short-range interactions: cation-anion, anion-anion, and cation-cation. Of each energy curve, the long-range Coulomb energy has been pre-subtracted from the total energy.

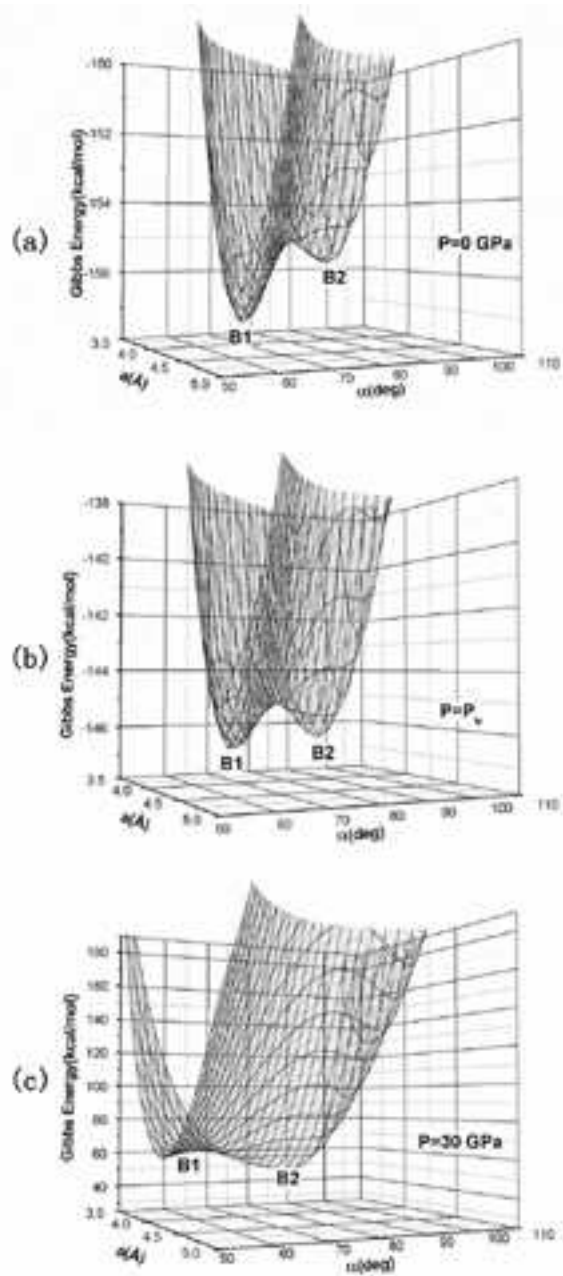


Fig. 2. The $0 - K$ Gibbs free energy surfaces of $R\bar{3}m$ symmetry at (a) zero, (b) P_{tr} and (c) $30 GPa$, respectively.

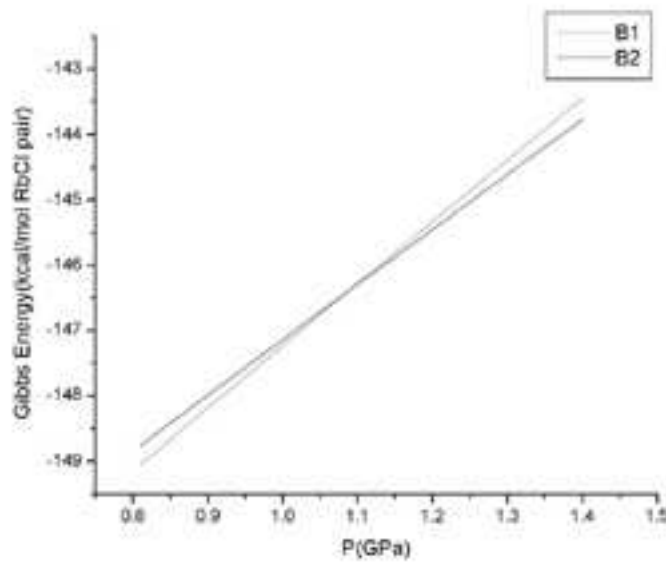


Fig. 3. The Gibbs free energies of relaxed B1 and B2-structure RbCl crystals increase with external pressure. The two curves have a crosspoint at $P = 1.09\text{GPa}$.

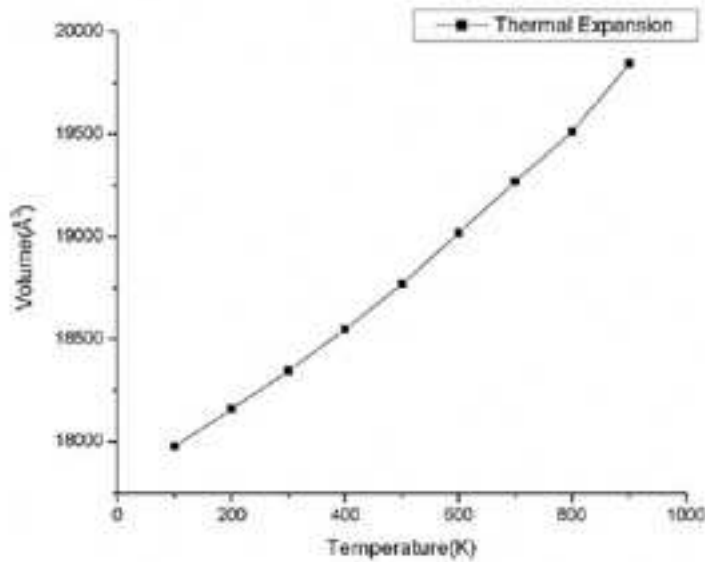


Fig. 4. The thermal expansion of perfect B1-RbCl crystal calculated with molecular dynamics. Temperature varies from 100K to 900K. The linear coefficient of thermal expansion is defined as $(1/L)(dL/dT)$, where L is the lattice constant, and the derivative is calculated as a central derivative with a temperature step of 200K.

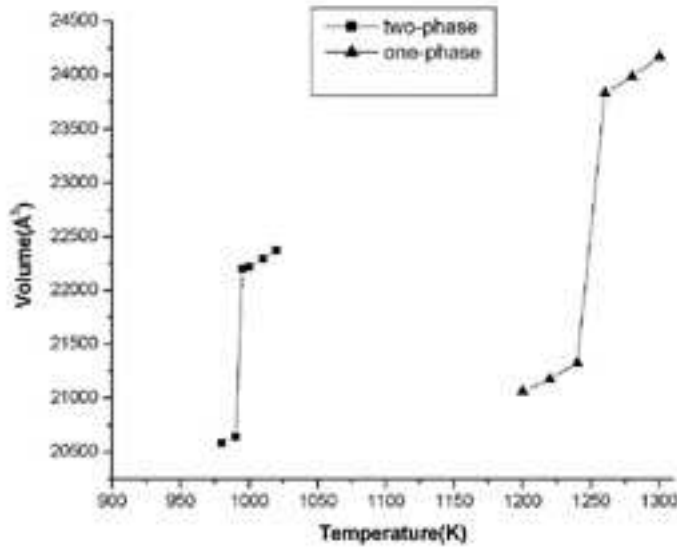


Fig. 5. The volume-temperature curves of the coexist-phase lattice and the perfect lattice. The abrupt change of volume with the one-phase method occurs at a temperature about 260K higher than that of the two-phase method.

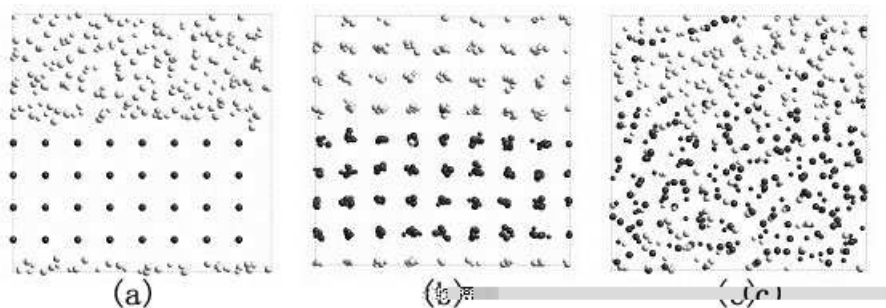


Fig. 6. The initial configuration of a coexist-phase lattice (a) and possible final configurations (b)(980K), (c)(1000K) after equilibrating the system at different temperatures. Dark circles refer to ions that were initially in the solid phase; gray circles refer to ions initially in the liquid phase. The system has almost completely solidified as (b); and has almost completely melted as (c).

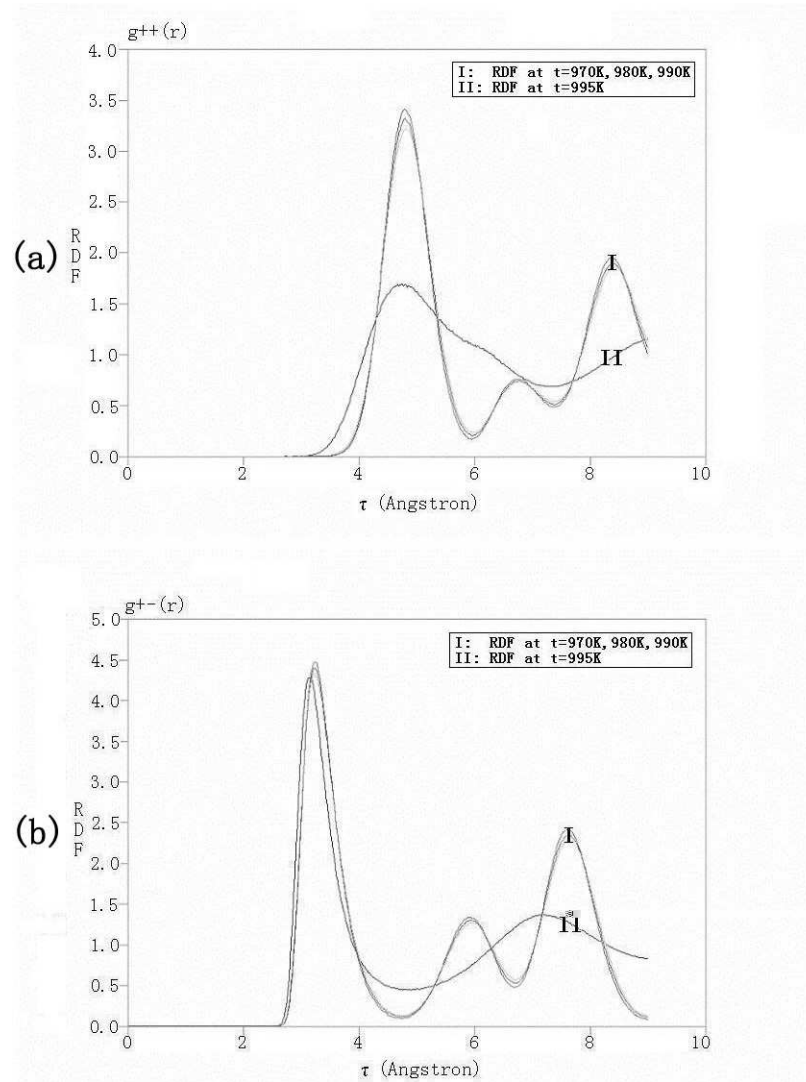


Fig. 7. The radial distribution function (RDF) of the final configurations at different temperatures. The abrupt change of RDF indicates the occurrence of melting. (a) shows the RDF of cation-cation and (b) shows that of cation-anion.

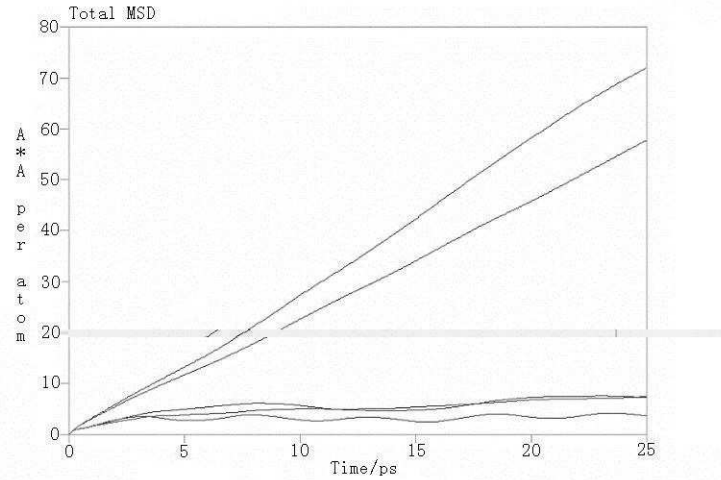


Fig. 8. The mean-square displacement (MSD) of all ions as the function of time at different temperatures. The change of MSD curves indicates the occurrence of melting: at low temperatures the MSD oscillates near its balance, while it increases with time at temperatures above melt-point.

	Lattice Constants (Å)			Cell Angles (°)			Lattice Energy (eV/RbCl)	Bulk Modulus (GPa)	Elastic Coefficient (GPa)		
	a	b	c	α	β	γ			C ₁₁	C ₁₂	C ₄₄
Experimental data	6.517	6.517	6.517	90	90	90	-7.03	18.5	36.4	6.3	4.7
Möbius inverse potentials	6.529	6.529	6.529	90	90	90	-6.85	19.0	43.0	5.0	5.0
Compass98_02 potentials	6.550	6.550	6.550	90	90	90	-7.16	19.6	44.1	7.4	7.4

Table II. Calculated and experimental properties of B1-RbCl crystal, a Compass98_02 model is also afforded for comparison. Experimental data all come from Ref.13.

Fig. 9. Table II.

Temperature (K)	200	300	400	500	600
Calculations (10^{-6}K^{-1})	33.7	35.1	38.1	42.0	43.9
Experimental data (10^{-6}K^{-1})	32.8	39.8	42.3	44.4	46.5

Table III. Calculated and experimental linear coefficient of thermal expansion at different temperatures

Fig. 10. Table III.